

Materials Selection for Use in Hydrochloric Acid

A.K. Mishra¹, N. Ebrahimi², D.W. Shoesmith² and P.E. Manning¹

¹Haynes International, Inc.
1020 West Park Avenue, Kokomo, IN 46904, US

² Department of Chemistry
Western University, London, ON, N6A 5B7, Canada

Abstract

Hydrochloric acid (HCl) is an important mineral acid with many uses, including the pickling of steel, acid treatment of oil wells and chemical cleaning and processing. This acid is extremely corrosive and its aggressiveness can change drastically depending on its concentration, the temperature and contamination by oxidizing impurities. One of the most commonly encountered oxidizing impurities is the ferric ion. In general, stainless steels cannot tolerate aggressive HCl solutions, hence the need to use corrosion-resistant nickel-based alloys.

A part of this study focused on the role of alloying elements on the corrosion performance of commercial nickel-based alloys C-276 (UNS N10276), C-22 (UNS N06022), C-2000 (UNS N06200), Alloy 625 (UNS N06625), Hybrid-BC1 (UNS N10362) and B-3 (UNS N10675) in HCl solutions, with and without the presence of oxidizing impurities (ferric ions). Aggressive HCl solutions can also be used to simulate the critical crevice solution. Therefore, another aspect of this research is to investigate the role of alloying elements in Nickel-based alloys on the inhibition of crevice corrosion. In the present study various standard corrosion test methodologies, conservative electrochemical techniques, and a range of surface analytical tools have been utilized.

Keywords: Nickel Alloys, Molybdenum, Hydrochloric Acid, Oxidants, Galvanostatic, Potentiodynamic, Crevice Corrosion, SEM, EDX, Surface Profilometer

Introduction

Hydrochloric acid (HCl) is an important mineral acid, second only to sulfuric acid (H₂SO₄) in its uses in industry. Major applications include acid pickling of steel, acid treatment of oil wells, chemical cleaning and processing, ore reduction, production of chlorine and chlorides and food

processing [1]. There is a very limited choice of materials for use in this solution, as, most of the commonly used metals and their alloys experience extensive general and/or localized corrosion attack in the HCl. Further, the solution aggressiveness drastically changes depending upon the concentration, temperature and the presence of oxidizing impurities (like ferric ions, cupric ions etc.).

Nickel-alloys containing optimum amounts of chromium (Cr), molybdenum (Mo) and tungsten (W) are widely used in the chemical process industries due to their tolerance to both oxidizing and reducing conditions [2]. Major alloying elements like Cr and Mo (or Mo + W) play a major role in maintaining the passivity of the alloy and stabilizing the passive film after a localized breakdown event [3]. Chromium forms the primary Cr_2O_3 passive film, which is dominantly responsible for passivation while Mo (and W) is known to inhibit localized corrosion by oxide reformation within initiated pits, thereby retarding their growth [4-6]. Despite their excellent general corrosion resistance, these alloys are prone to localized corrosion (particularly crevice corrosion) in extremely aggressive environments [7].

Meck et al. [8] studied the corrosion performance of N10675 (Ni-Mo alloy) and N06200 (Ni-Cr-Mo-Cu) alloys in reagent grade HCl acid, with and without the presence of impurities, using an electrochemical technique. In the reagent grade HCl solution, N10675 alloy demonstrated a high corrosion resistance. However, in the presence of oxidizing impurity, the corrosion resistance of N06200 was significantly higher compared to N10675 alloy. The results are in consensus with the weight loss data [2].

In this study, the role of alloying elements in a number of commercially-available nickel-based alloys was evaluated in several aggressive environments using weight loss and electrochemical measurements in conjunction with the surface characterization techniques.

Experimental

Corrosion tests were conducted on C-2000 (UNS N06200), Alloy 59 (UNS N06059), C-22 (UNS N06022), C-22HS (UNS N07022), Alloy 625 (UNS N06625), C-276 (UNS N10276), HYBRID-BC1 (UNS N10362) and B-3 (UNS N10675) alloys. The nominal compositions of the studied alloys are shown in Table 1.

Corrosion Tests

Immersion Technique

Corrosion tests of the wrought alloys were carried out under laboratory conditions using glass flask/condenser systems and reagent grade chemicals. The sample dimensions were 25 x 25 x 3 mm. The surfaces of these samples were ground using 120 to 600 grit papers, then de-greased with acetone, prior to weighing and then testing of the samples. A test duration of 96h was selected, with interruptions every 24h to weigh the samples. The solution used was concentrated HCl acid. Corrosion studies were performed in HCl solutions to which various amounts of oxidizing impurity had been added.

Electrochemical Techniques

For electrochemical measurements, specimens with a total surface area of ~ 14 cm² were cut from the plate materials. A small tapped hole was machined in the top of the specimen to enable contact, via a cylindrical rod, to external circuitry. This rod was sheathed in glass and sealed with a polytetrafluoroethylene (PTFE) gasket to prevent contact with the electrolyte. The sample was then polished with a series of wet silicon carbide papers up to 600 grit, rinsed with deionized water and acetone, and then air dried prior to an experiment. A platinum (Pt) foil and a saturated calomel electrode (SCE) were used as the counter and reference electrode, respectively.

The electrochemical tests were performed in deaerated 20% HCl at various temperatures. The open circuit potential (OCP) was recorded for 1h to allow a near steady-state value to be approached. Subsequently, linear polarization resistance (LPR) measurements were conducted as per ASTM¹ G-59 [9], from -20 to +20 mV of the E_{corr} . Potentiodynamic polarization (PP) tests were performed from -250 mV below E_{corr} to +1100 mV above at a scan rate of 0.167mV/s in the forward direction. To study the effects of impurities in HCl on the corrosion behavior, electrochemical experiments (OCP, LPR and PP) were conducted in 20% HCl containing various concentrations of Fe^{3+} ions.

For the crevice corrosion study, two different crevice arrangements were used: (a) a Multiple Crevice Assembly (MCA) and (b) a Single Crevice Assembly (SCA). The experimental details and the electrochemical techniques utilized when using these arrangements have been reported elsewhere [7, 10, 11, 12]. The electrolyte used for crevice corrosion experiments was 1M NaCl. In SCA, the temperature selected was 105°C and a galvanostatic current of 20 μ A was applied to guarantee crevice initiation and to control its propagation. In MCA experiments the potentiodynamic-galvanostatic-potentiodynamic (PD-GS-PD) technique [7, 11] was used at 80°C since the primary goal of the experiments was to measure breakdown and repassivation potentials and critical temperatures [7].

Table 1. Nominal alloy compositions (wt. % of major alloying element)

Alloys	Cr	Mo	W	Cu	Ni
UNS N06200	23	16		1.6	Bal.
UNS N06059	23	16			Bal.
UNS N06022	22	13	3		Bal.
UNS N07022	21	17			Bal.
UNS N06625	21	9			Bal.
UNS N10276	16	16	4		Bal.
UNS N10362	15	22			Bal.
UNS N10675	1.5	28.5			Bal.

Characterization Techniques

Electrodes anodically oxidized for surface analyses were rinsed gently with DI water and air dried prior to characterization. XPS analyses were performed with a Kratos² Axis Ultra XPS at Surface Science Western (SSW)¹ employing monochromatic Al K_{α} (1486.8 eV) radiation. The binding energy was calibrated to give a Au 4f_{7/2} line position at 83.95 eV. XPS spectra were corrected for charging by taking the C 1s spectrum for adventitious carbon to be at a binding energy of 284.8 eV. Survey spectra were recorded on all samples followed by high resolution XPS spectra for Ni

¹ American Society for Testing and Materials (ASTM), 100 Barr Harbor Drive, West Conshohocken, PA 19428-2959

² Trade Name

2p, Cr 2p, Mo 3d, W 4f, C 1s and O 1s spectral regions. The SEM images of the creviced corroded specimens were obtained on a LEO³ 440 SEM equipped with an EDAX¹ EDX system. The depth of penetration and images of the corroded region were obtained using surface profilometry.

Results

The corrosion rate (in mils per year), obtained from weight change measurements, in various concentrations of HCl acid are shown in Figure 1. The rates for N10675 and N10362 are the lowest over a wide range of HCl concentrations. Based on their corrosion resistance performance in HCl at the studied temperatures, the alloys can be ranked (high to low) as,

$$\mathbf{N10675 > N10362 > N10276 > N06200 > N06022} \quad (1)$$

The ranking follows the same trend as the amount of Mo in the respective alloys, which decreases in the same sequence from N10675 (28.5%, wt.%) and lowest in N06022 (13%, wt.%). It must be taken into consideration that even though both Mo and W behave similarly but Mo demonstrates a better corrosion resistance than W, in low pH reducing solutions, for a similar concentration (in wt.%). The effect of temperature on the corrosion rate in HCl was also investigated, as shown in Figure 2. As observed in Figure 1, the corrosion rate of N10675 was the lowest across the whole temperature range.

At higher temperatures (like $T > 60^{\circ}\text{C}$), where the solution aggressiveness increases significantly, the corrosion rate is still low for the N10675 and N10362 alloys. Based on this corrosion data, N10675 can be selected as the most corrosion resistant alloy, followed by N10362 alloy for application in reagent grade HCl.

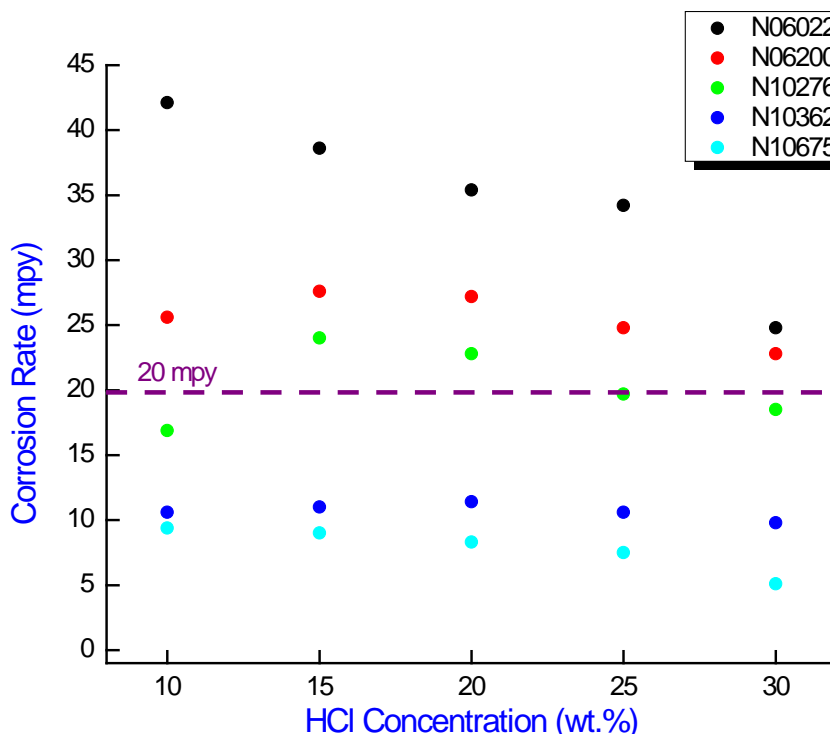


Figure 1. Corrosion rates of a number of Ni-based alloys in HCl at 66°C obtained from weight change measurements.

¹ Trade Name

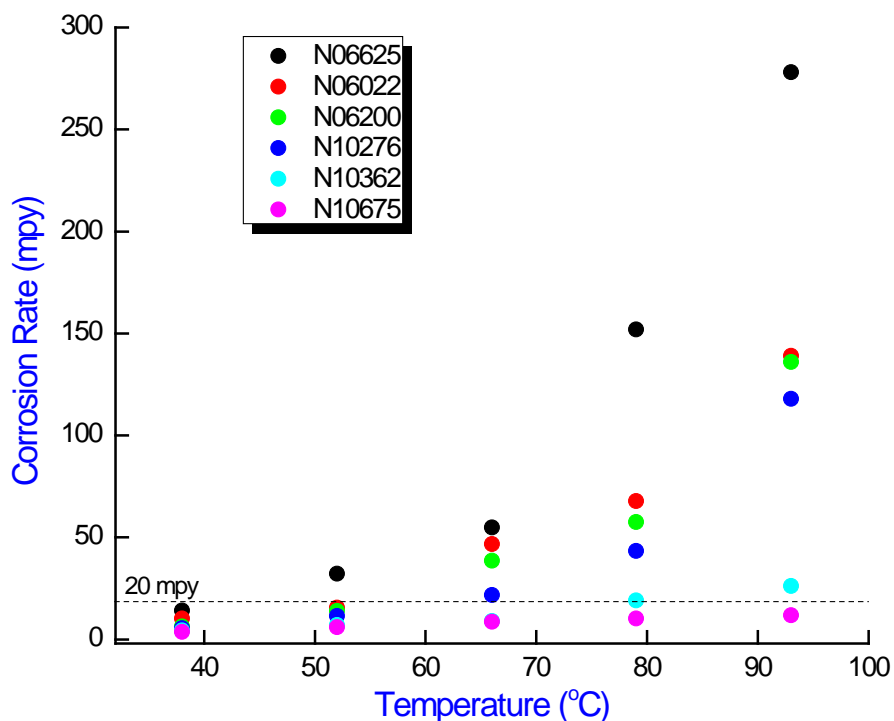


Figure 2. Corrosion rates of a number of Ni-based alloys in 20% (wt.%) HCl at various temperatures obtained from weight change measurements.

Since industrial HCl acid is not similar to reagent grade due to the presence of impurities (primarily Fe^{3+} ions) in the former, the role of Fe^{3+} on corrosion in HCl acid was investigated. Corrosion rates were obtained in 20% HCl at 52°C, with and without the presence of Fe^{3+} , Figure 3. In the absence, or when only a very small concentration (10 ppm) of Fe^{3+} was present in the HCl, the corrosion rate was lowest for N10675 and highest for N06022 alloy. However, when the concentration of Fe^{3+} was high (1000ppm) the corrosion rate was highest for N10675 and lowest for N06200.

The corrosion resistance performance of various CRA's can be ranked (high to low) as:

In 20% HCl at 52°C

$$N10675 > N10362 > N10276 > N06200 > N06022 \quad (2)$$

In 20% HCl + 10 ppm Ferric ions at 52°C

$$N10675 > N10362 > N10276 > N06200 > N06022 \quad (3)$$

In 20% HCl + 1000 ppm Ferric ions at 52°C

$$N06200 > N06022 > N10276 > N10362 > N10675 \quad (4)$$

Based on the corrosion data in 20%HCl solution, with and without the addition of ferric ions (eqn. 2-4), it can be concluded that a Nickel-based alloy containing high Mo (N10675 alloy in the present study) will demonstrate the best corrosion resistance in HCl acid. However, in presence of high concentrations of impurity, an alloy containing high Cr (N06200 alloy in the present study) (Table 1) will experience the lowest corrosion attack.

To better understand the corrosion mechanism, electrochemical tests were conducted in 20%HCl and 20%HCl + Fe^{3+} ions. The polarization resistance (R_p) values, determined using the LPR technique, Figure 4, show a similar trend in corrosion resistance performance of various alloys in 20%HCl acid (with and without the presence of Fe^{3+} ions) as observed from the weight

loss measurements. The potentiodynamic polarization graphs (Figure 5) recorded in 20% HCl clearly showed a strong relationship between alloy Cr content and the passivation current density with a high amount of Cr resulting in a low passivation current density (i_p). A low i_p can be attributed to the presence of a protective and less defective passive film. The potentiodynamic polarization study showed no passive film was formed on N10675 (Table 1). Since, Fe^{3+} is a strong oxidant, the absence of a passive film resulted in a high corrosion rate on N10675 in 20% HCl + 1000 ppm Fe^{3+} (Figure 3).

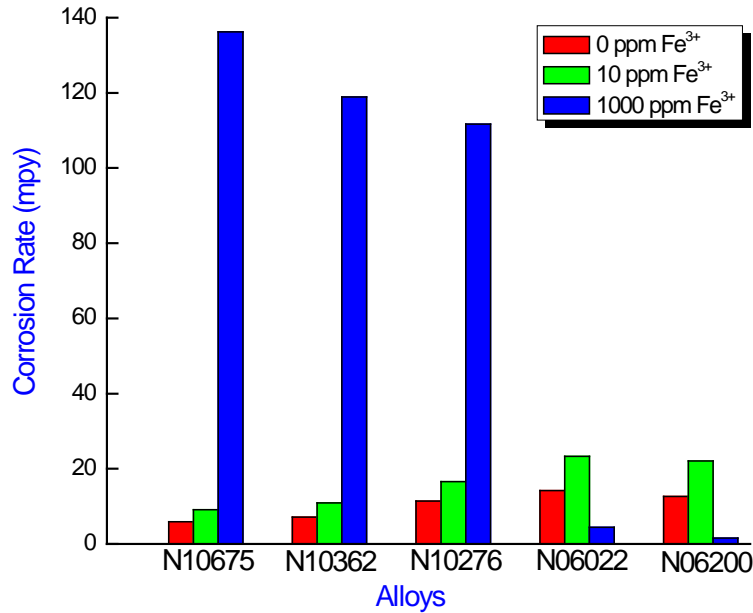


Figure 3. Corrosion rates of various alloys in 20% (wt.%) HCl acid, with and without added Fe^{3+} , at 52°C obtained from weight loss technique

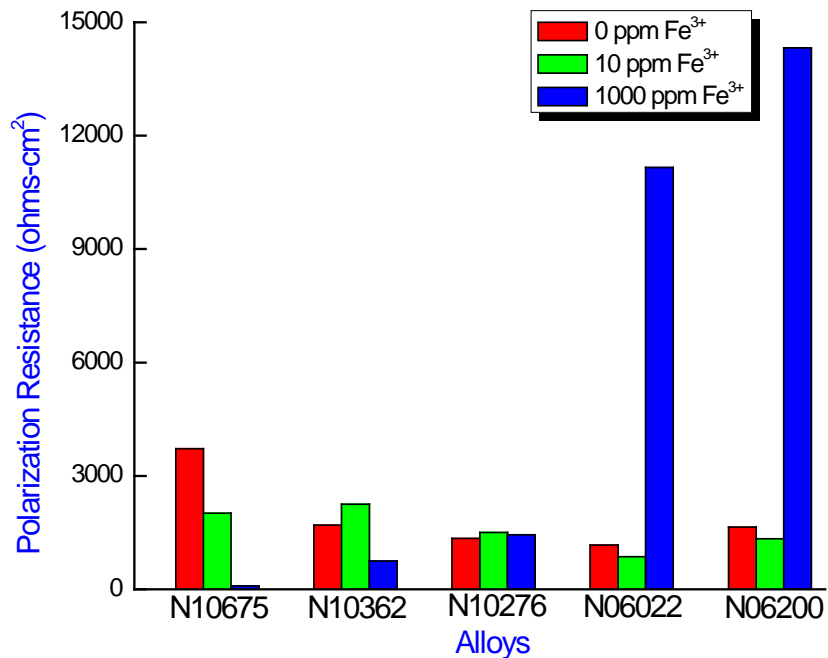


Figure 4. Polarization resistance (R_p) of various alloys in 20% (wt.%) HCl acid, with and without added Fe^{3+} , at room temperature

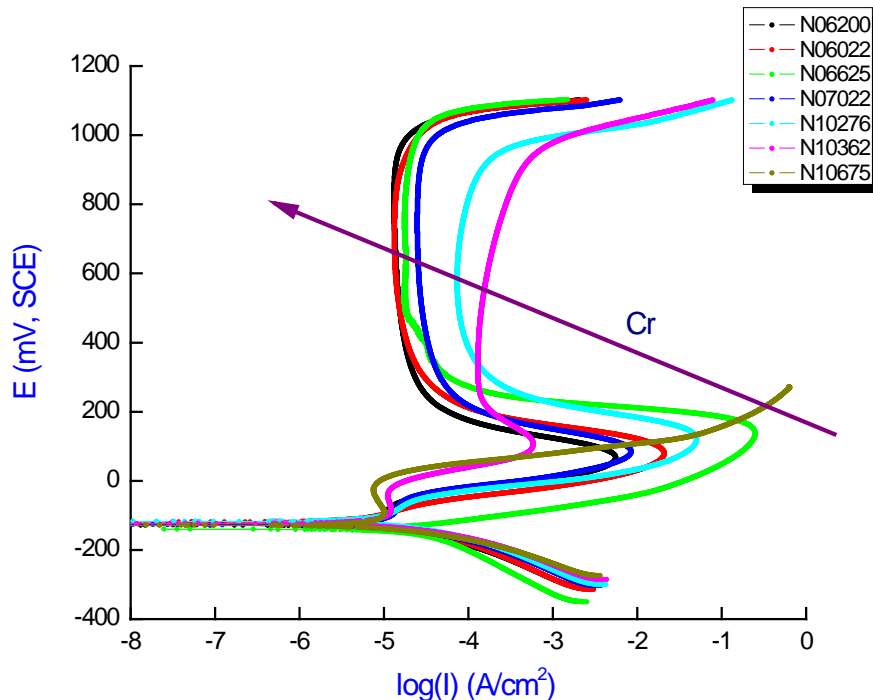


Figure 5. Potentiodynamic polarization curves in 20% (wt.%) HCl at an ambient temperature

Electrochemical tests were also performed in HCl at various temperatures, Figures 6 and 7. With an increase in the temperature from ambient to 52°C, both the passivation current density (i_p) and the corrosion current density (i_{corr}) increases by almost an order of magnitude for N06022 (Figure 6). Since i_{corr} is directly proportional to the corrosion rate, this indicates an increase in corrosion rate with temperature for N06022. However, in a similar environment for N10362, i_p increases by more than an order of magnitude, while i_{corr} showed little change, Figure 7, in agreement with the weight loss data, Figures 1 and 2. This independence of corrosion rate on concentration and temperature for Mo enriched alloys suggests the formation of a protective oxide film of Mo which plays a major role in maintaining passivity. Based on these studies, the most suitable alloy for use in reagent grade concentrated HCl are N10675 and N10362.

OCP curves recorded on N06022 and N10362 in 20% HCl, with and without the presence of Fe^{3+} , are shown in Figures 8 and clearly demonstrate the oxidizing nature of Fe^{3+} ions. A schematic illustrating the role of oxidants (Fe^{3+}) on the corrosion performance of Ni-based alloys is shown in Figure 9. The figure includes two polarization curves, one for a low Mo (Mo + W)-high Cr alloy (black curve) and one for a high Mo (Mo + W)-low Cr alloy (red curve). A sufficient concentration of added Fe^{3+} (leading to the cathodic current potential relationship indicated by the blue line) will lead to an OCP in the passive region as indicated by the intersection of the blue line with the two polarization curves. Under these conditions, the passive current (and hence the corrosion rate) would be lower on the high Cr alloy (indicated by the green arrow). However, if the Fe^{3+} concentration was less than the critical current density (the peak current during the active to passive transition), the blue line would eventually shift to lower potentials and into the active region as indicated by the blue arrows (with C_o indicating the decrease in oxidant concentration). Under these conditions, consistent with our observations, the corrosion rate would be expected to decrease as the Mo (Mo + W) content of the alloy increased. The presence of ferric ions in HCl solution, or any aqueous solution, simply influences the overall cathodic reaction due to the reduction of ferric ions to a lower oxidation state. Thus, among Ni-Cr-Mo (W) alloys, an alloy

having higher amount of Cr will demonstrate a better corrosion resistance in HCl solution containing moderate to high amount of ferric ions.

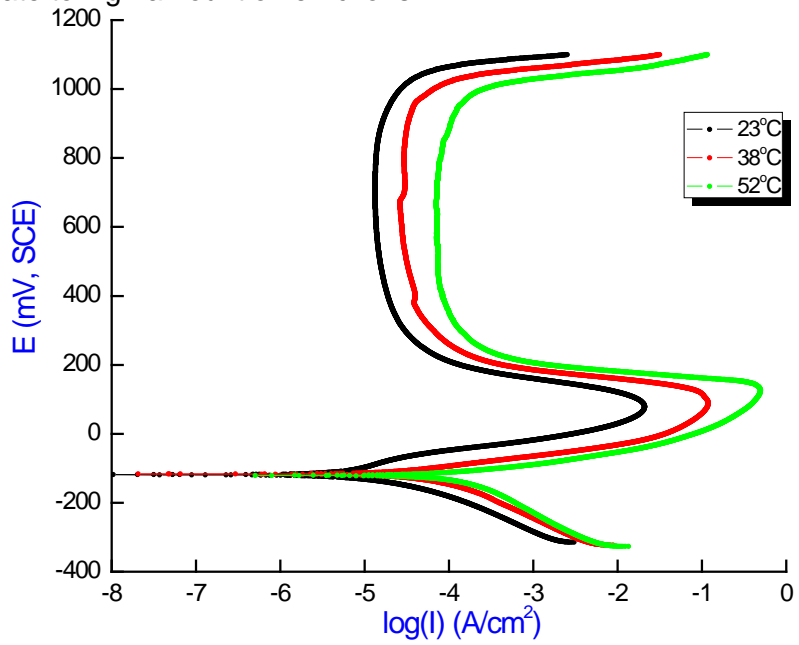


Figure 6. Potentiodynamic polarization curves recorded on N06022 in 20% (wt.%) HCl at various temperatures

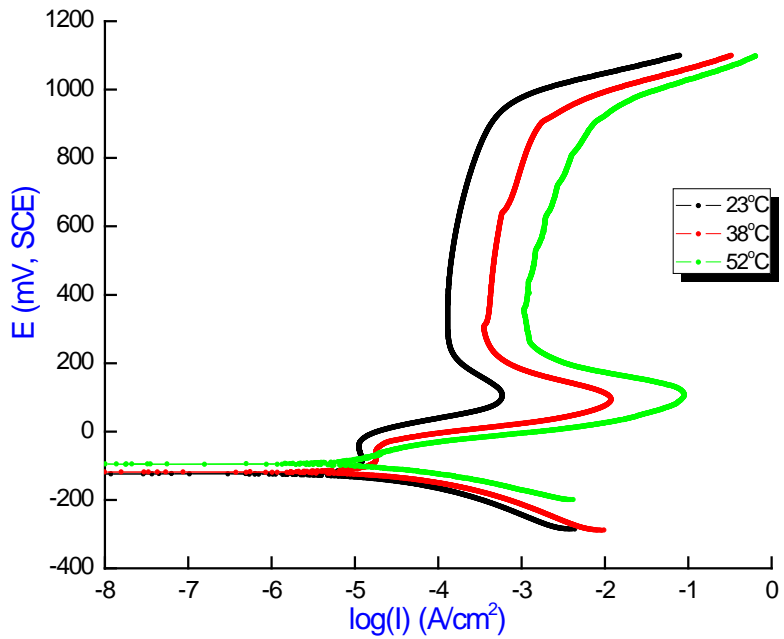
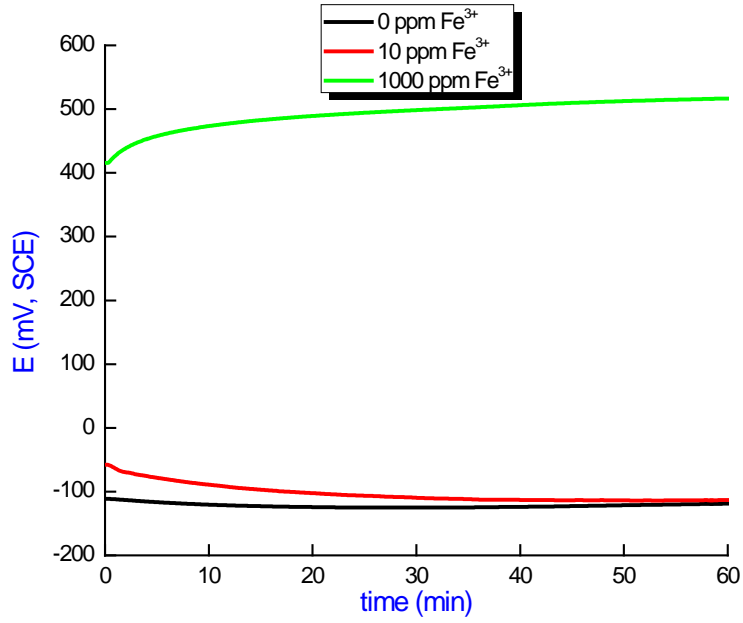
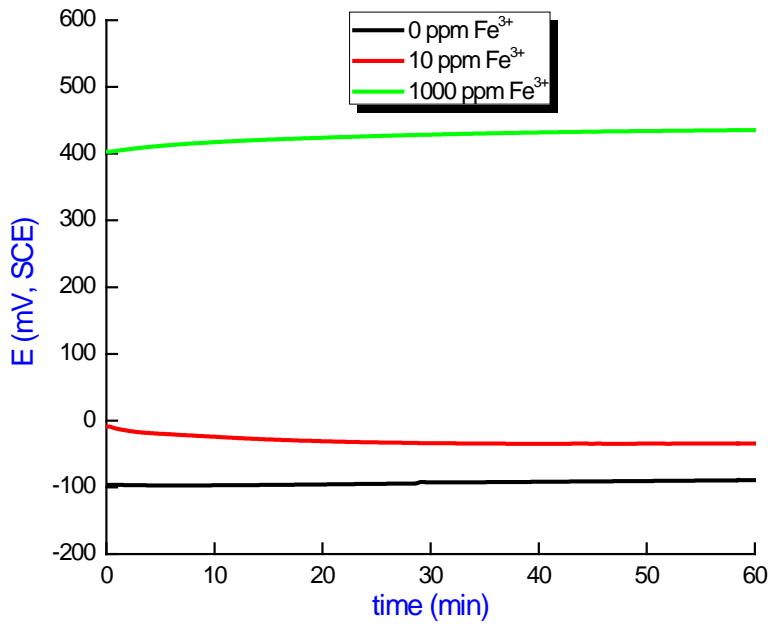


Figure 7. Potentiodynamic polarization curves recorded on N10362 in 20% (wt.%) HCl at various temperatures



(a)



(b)

Figure 8. OCP in 20% (wt.%) HCl, with and without added Fe³⁺ impurity, at an ambient temperature for (a) N06022 and (b) N10362

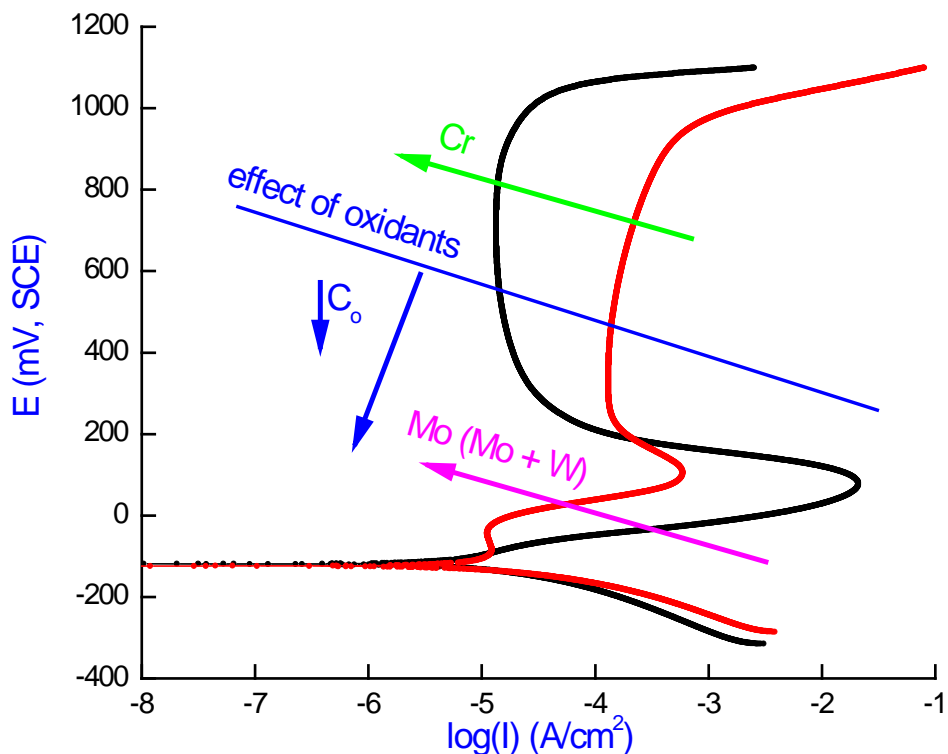


Figure 9. Schematic of effect of oxidants on the corrosion performance of Ni-Cr-Mo (W) alloys

Another interesting observation in the PP curves in HCl solution is the anodic current behavior in the active region (i.e., between the corrosion potential and the active-passive transition) for alloys enriched in Mo (or Mo + W) (Figures 5 and 9). The current arrest at potentials lower than the active to passive transition indicates a distinct suppression of active dissolution as the Mo (Mo + W) content is increased as observed in Figure 5 and 9.

XPS technique was used to analyze the composition of the oxide films present after either natural corrosion (for 5h) or potentiostatic polarization in the passive region (500 mV vs SCE; hold time as 5h) in 20% HCl. For comparison the composition of the native oxide (i.e., that form by air exposure) was also determined. Figure 10 shows the atomic concentration (expressed as at. % of cation content) obtained from XPS survey spectra.

In the air-formed film the Cr is enriched as expected but the film is dominated by the Ni content on both alloys. In the passive region both alloys are enriched in Cr and depleted in Ni in particular the high Cr-containing N06022 alloy confirming that the low passive current density measured on this alloy (Figure 5) is due to Cr enrichment. There is also a slight enrichment in Mo content but this is slight considering the difference in Mo content in the two alloys. Under natural corrosion conditions the surface of both alloys is strongly depleted in Ni but enriched in Mo not Cr. This enrichment is slightly greater for the high Mo N10362 than the lower Mo (+W) containing N06022. Although the differences in Mo content on the surfaces of the two alloys is relatively small this enhancement is consistent with the relative small difference in corrosion rates between the two alloys measured by weight loss at low temperatures, Figure 2.

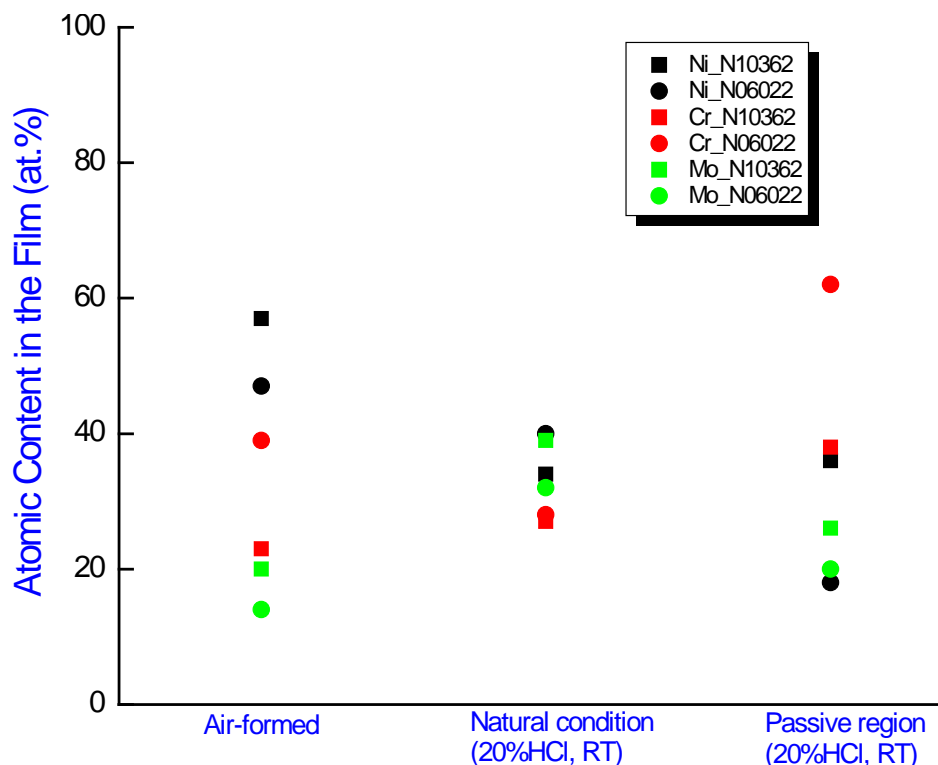


Figure 10. Atomic concentration of major alloying elements obtained from XPS survey spectra

While Ni-Cr-Mo (W) alloys are generally not susceptible to pitting, crevice corrosion remains a possibility under sufficiently aggressive conditions [7]. To investigate the conditions that could apply under active crevice conditions, crevice corrosion was forced to initiate using an applied current of 20 μ A. Figure 11 shows the potential-time curve recorded on N06022 in 1M NaCl at 105°C using the single crevice arrangement (SCA). The initiation of crevice corrosion is indicated by the ~ 400 mV drop in potential over the period 5 to 7 hours. Optical micrographs of the crevice corroded region after an exposure period of 48 h are shown in Figure 12. The optical micrograph in Figure 12a shows the sharp boundary between the non-creviced and creviced regions. In the creviced region, many deep and connected pits are observed on the grain boundaries and smaller less developed pits on the individual grain surfaces, Figure 12(b).

As observed in Figures 12 (a) and (b), not all the grain boundaries in the heavily corroded region suffered intergranular corrosion. This is consistent with the observations of Jakupi et al. [14] who showed that, on N06022, localized corrosion preferentially initiated at triple points and non- Σ 3 grain boundaries. The observations of Jakupi et al. were on more lightly crevice corroded specimens in experiments conducted at a lower temperature (70°C). At the higher temperature of 105°C employed in this study, pit growth is more rapid and grain boundary selectivity less marked.

Figure 13 shows an SEM image of a creviced corroded region on N06022 near the crevice edge and a series of EDX maps for the various alloy constituents. The interlinked pits along the grain boundaries contain corrosion product deposits, enriched in Mo, W and O and depleted in Ni and Cr, consistent with previous observations [12, 15] and indicating that pit propagation is controlled by the deposition of Mo and W as a result of the local acidity arising at these active locations. Jakupi et al. [12] used Raman spectroscopy to show that Mo and W form as polymeric molybdates and tungstates in crevice corroded locations on N06022. If it is accepted that 20% HCl is a reasonable surrogate for the critical crevice solution existing within the active locations within the crevice then the accumulation of Mo, in the form of molybdates, would be expected at

these active pit locations. Since the corrosion rate should then be decreased corrosion penetration at these locations should be limited.

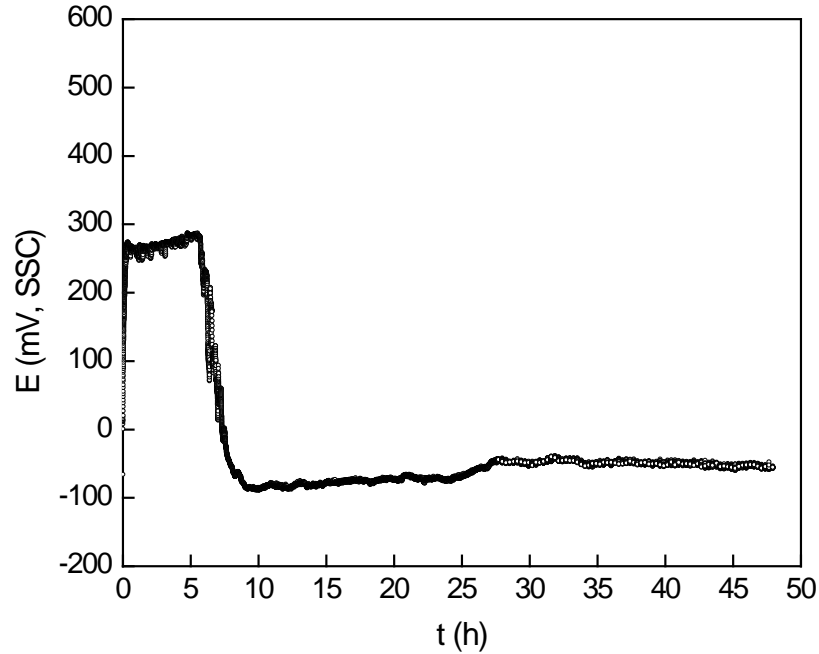


Figure 11. Potential-time curve recorded on N06022 at an applied current of 20 μ A in 1M NaCl (105°C) using the single crevice arrangement

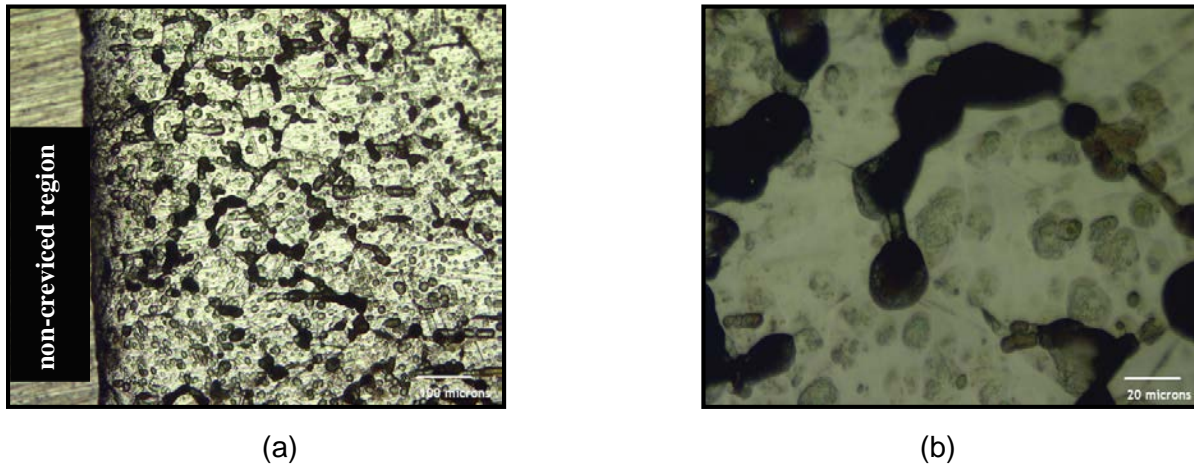


Figure 12. Optical micrographs of the crevice corroded region on N06022 at different magnifications after the experiment described in Figure 11: (a) 100X and (b) 500X

To examine whether this was the case the crevice corrosion damage sustained on the N06625 (9wt% Mo) and the N06059 (16 wt%Mo) alloys was compared since both have similar Cr contents and neither alloy contains W (Table 1). Figure 14 shows the depth profiles and line scans measured using a profilometer on the crevice corroded region. The specimens examined were from previous PD-GS-PD experiments performed in 1 M HCl at 80°C using the MCA. The maximum depth of penetration is greater on N06625 (~30-35 μ m) than on N06059 (~2.5-3 μ m). These results are consistent with those of Kehler and Scully [16] who used confocal laser scanning microscopy to show that the depth of penetration due to crevice corrosion was higher

for alloy N06625 than for N06022 (13 wt% Mo + 3 wt% W, Table 1), and confirm the role of Mo in suppressing alloy corrosion under active highly acidic conditions. Additionally, inspection of the profiles and line scans (Figure 14) shows that corrosion damage is uniformly distributed around the mouth of the crevice on alloy N06059, but highly localized at one edge on N06625.

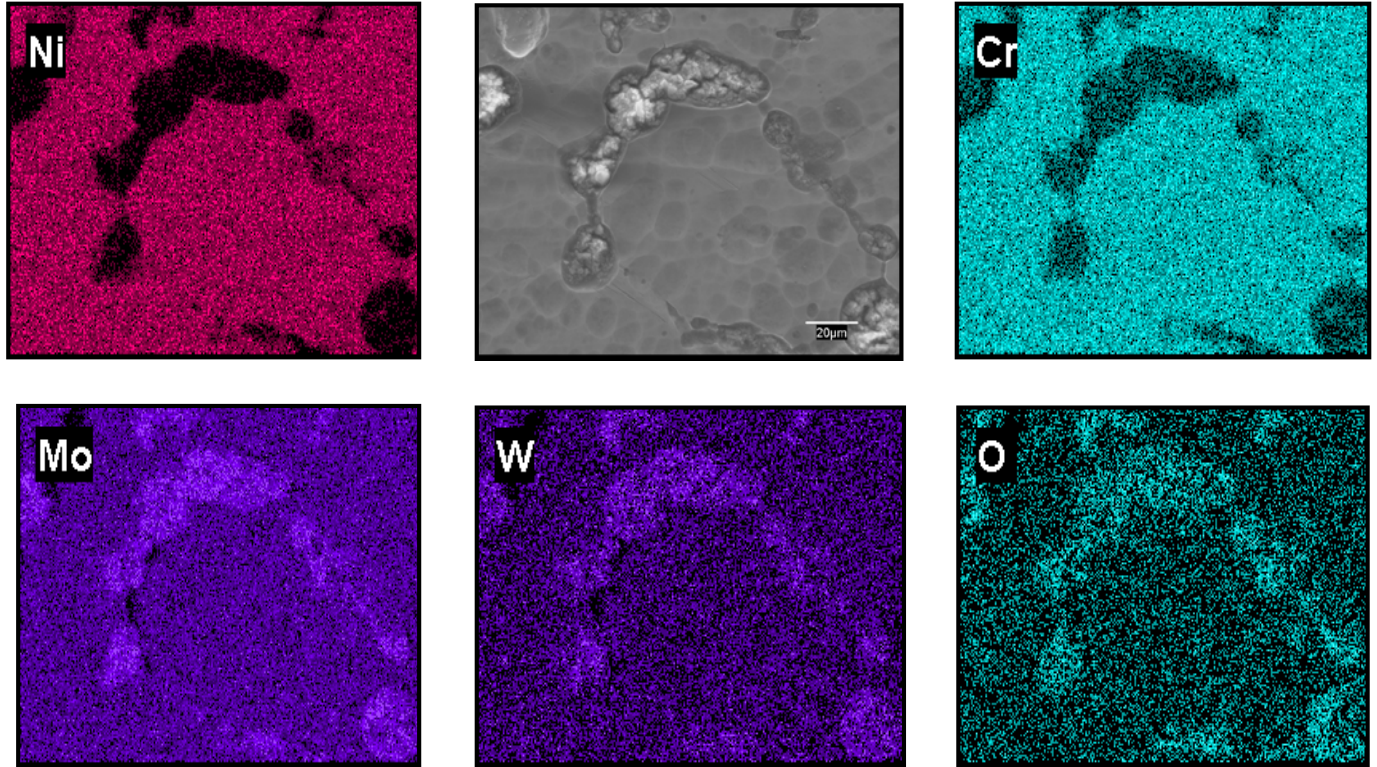
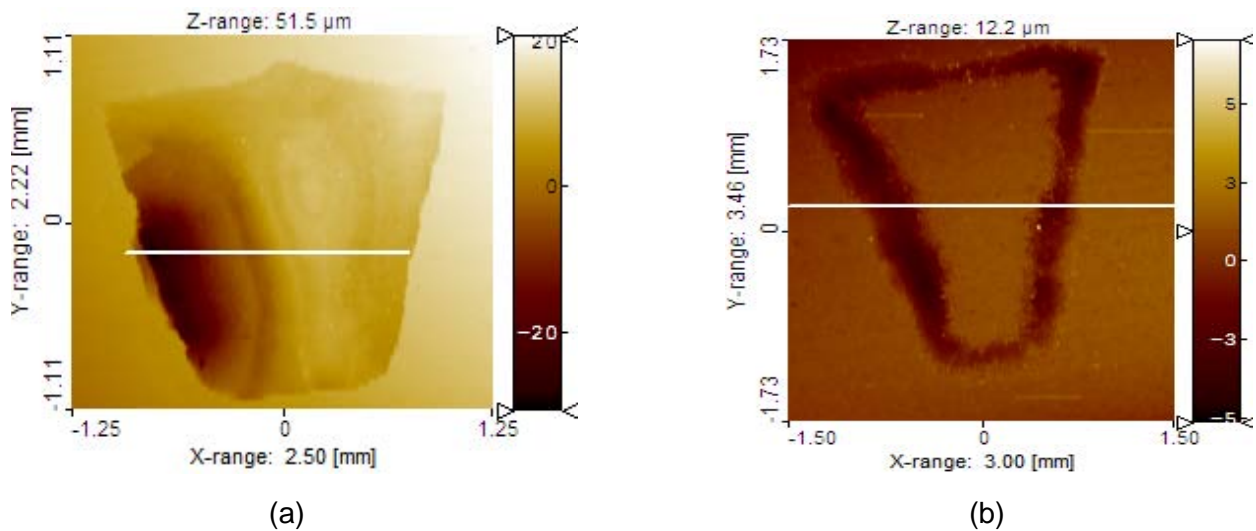
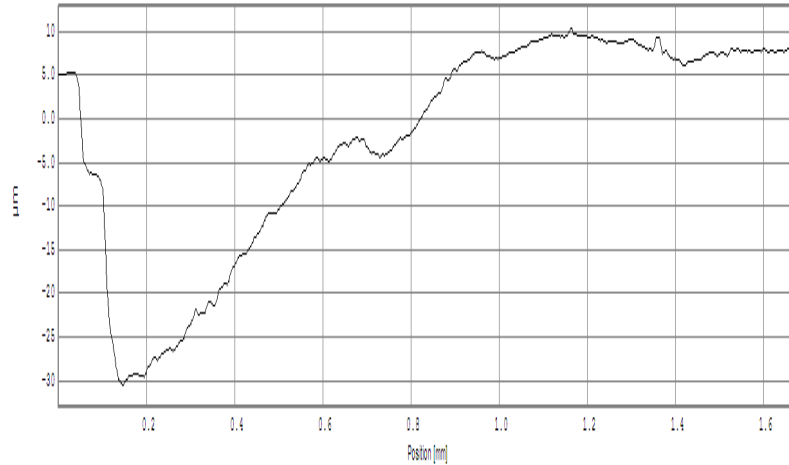
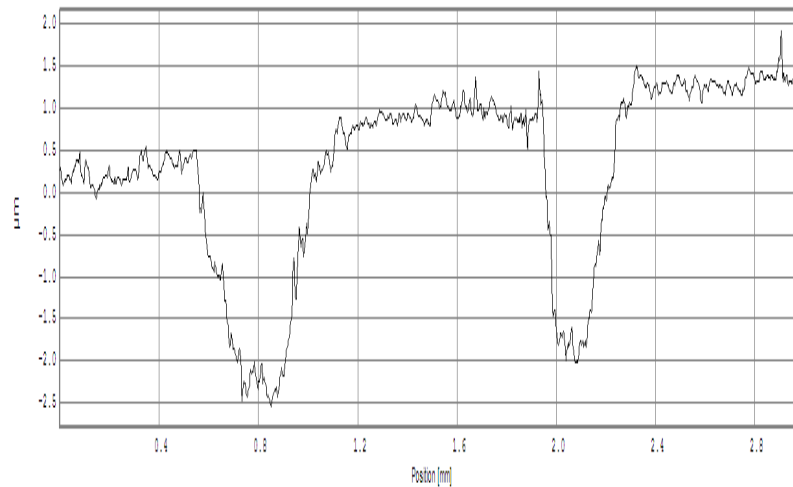


Figure 13. SEM micrograph and EDX maps of the crevice corroded region on N06022 showing the Mo/W/O corrosion product deposits formed on the grain boundaries





(c)



(d)

Figure 14. 2-D images of the creviced regions on recorded after a PD-GS-PD experiment at 80°C in 1.0 mol.L⁻¹ NaCl for (a) N06625 and (b) N06059; (c) depth profile recorded along the line shown in (a) for N06625, (d) depth profile recorded along the line shown in (b) for N06059

Since these experiments were conducted under constant current conditions, propagation is supported and repassivation prevented. Under these conditions, enforced propagation penetrates deep into alloy N06625 at the location at which crevice corrosion initiates since the Mo content is too low to build up the molybdate deposits required to prevent it. By contrast, on alloy N06059 penetration is limited by the accumulation of molybdates at the initiation site forcing propagation to proceed laterally around the outer edge of the crevice. These observations are consistent with those of Jakupi et al. [17] who showed that the depth of penetration of crevice corrosion on N06022 was dependent on the current applied, the rate of molybdate formation increasing at higher currents forcing lateral propagation and limiting the depth of propagation.

Conclusions

- Ni-based alloys containing high Mo (like N10675, N10362) demonstrate the highest corrosion resistance in reagent grade concentrated HCl solutions. In the presence of moderate to high levels of oxidizing impurity (Fe^{3+}), an alloy with a high Cr content (N06200, N06022) is required to maintain a low corrosion rate.
- Under natural conditions the surface oxide which provides protection against corrosion in concentrated HCl is enriched in Mo.
- The distribution and extent of crevice corrosion damage depends strongly on the Mo (Mo + W) content of the alloy
- On alloys containing only a small Mo (Mo + W) content (e.g., N06625 (9Mo)) the crevice propagation penetrates deep into the alloy at the initiation site
- On an alloy with a higher Mo (Mo + W) content (e.g., N06022 (13Mo + 3W)), propagation occurred as a series of interlinked shallow pits along grain boundaries, with the depth of penetration in any individual pit being limited by the accumulation of molybdates and tungstates

Acknowledgements

The authors greatly acknowledge the support from Surface Science Western (SSW) at Western University, Canada for surface characterization. Also, the author acknowledge the efforts of Corrosion technician Jeff Dillman and Danielle Richesin from Haynes International in conducting the corrosion tests.

References

1. MTI Publication MS-3, *Materials Selector for Hazardous Chemicals*, Vol. 3, *Hydrochloric Acid, Hydrogen Chloride and Chlorine*, Materials Technology Institute of the Chemical Process Industries, Inc. (Ed.: C.P. Dillon and W.I. Pollock, 1999)
2. P. Crook, N. S. Meck, J. Crum and R. B. Rebak, "Corrosion of Nickel and Nickel – Base Alloys", *ASM handbook 13B* (2005): pp. 228 – 251
3. J. R. Hayes, J. J. Gray, A. W. Szmodis and C. A. Orme, "Influence of Chromium and Molybdenum on the Corrosion of Nickel-Based Alloys", *Corrosion* 62 (2006): p. 491
4. M. Moriya and M. B. Ives, "The Structure of Anodic Films Formed on Nickel and Nickel-13 w/o Molybdenum Alloy in pH 2.8 Sodium Sulfate Solution", *Corrosion* 40 (1984): p. 62
5. M. Moriya and M. B. Ives, "Surface Segregation of Molybdenum during Pitting Corrosion of a Nickel-Molybdenum Alloy", *Corrosion* 40 (1984): p. 105
6. R. Qvarfort, "Some Observations Regarding the Influence of Molybdenum on the Pitting Corrosion Resistance of the Stainless Steels", *Corrosion Science* 40 (1998): p. 215
7. A.K. Mishra and D.W. Shoesmith, "Effect of Alloying Elements on Crevice Corrosion Inhibition of Nickel-Chromium-Molybdenum-Tungsten Alloys Under Aggressive Conditions: An Electrochemical Study", *Corrosion* 70 (2014): p. 721
8. N.S. Meck, P. Crook and D.L. Klarstrom, "Effect of Ferric Ions on the Corrosion Performance of Nickel Alloys in Hydrochloric Acid Solutions", *Corrosion/2004*, paper no. 04430 (NACE International, Houston TX, 2004)
9. ASTM Annual Book of Standards, Volume 03.02 "Wear and Erosion, Metal Corrosion", (West Conshohocken, PA)
10. A.K. Mishra and D.W. Shoesmith, "Effect of Copper on Crevice Corrosion Inhibition of Nickel-Chromium-Molybdenum Alloy in Aggressive Conditions", *Corrosion/2015*, paper no. 5799 (NACE International, Houston TX, 2015)
11. A.K. Mishra and G.S. Frankel, "Crevice Corrosion Repassivation of Alloy 22 in Aggressive Environments", *Corrosion* 64 (2008): p. 836
12. P. Jakupi, F. Wang, J.J. Noel and D.W. Shoesmith, "Corrosion Product Analysis on Crevice Corroded Alloy 22 Specimens", *Corrosion Science* 53 (2011): p. 1670
13. D. A. Jones, *Principles and Prevention of Corrosion*, 2nd ed., (Upper Saddle River, NJ: Prentice Hall, 1996)
14. P. Jakupi, J.J. Noel, D.W. Shoesmith, "Intergranular Corrosion Resistance of Σ 3 Grain Boundaries in Alloy 22", *Electrochemical and Solid-State Letters* 13 (2010): p. C1
15. X. Shan, J.H. Payer, "Characterization of the Corrosion Product of Crevice Corroded Alloy 22", *Journal of Electrochemical Society* 156 (2009): p. C313
16. B. A. Kehler, J. R. Scully, "Role of Metastable Pitting in Crevices on Crevice Corrosion Stabilization in Alloy 625 and 22", *Corrosion* 61 (2005): p. 665
17. P. Jakupi, J.J. Noel, D.W. Shoesmith, "The Evolution of Crevice Corrosion Damage on the Ni-Cr-Mo-W Alloy 22 Determined by Confocal Laser Scanning Microscopy", *Corrosion Science* 54 (2012): p. 260